Appl Phys A (2014) 114:453–457
DOI 10.1007/s00339-013-7664-9

Applied Physics A
Materials Science & Processing

Possibility of room-temperature multiferroism in Mg-doped ZnO

Parmod Kumar · Yogesh Kumar · Hitendra K. Malik · S. Annapoorni · Sanjeev Gautam · Keun Hwa Chae · K. Asokan

Received: 5 February 2013 / Accepted: 10 March 2013 / Published online: 28 March 2013

Abstract Room-temperature multiferroic properties in Mg-doped ZnO samples are reported wherein Mg replaces Zn in the ZnO matrix and retains hexagonal wurtzite structure. The saturation magnetisation is increased from $\sim 2 \times 10^{-4}$ emu/g to 3×10^{-4} emu/g for the dilute doping of 2 % Mg in pure ZnO and the ferroelectricity is also increased. Higher concentration of Mg does not lead to a significant enhancement in the magnetisation but improves the ferroelectric properties. An X-ray absorption spectroscopic study shows an enhancement in O vacancies with dilute doping of Mg. The origin of the multiferroic behaviour is understood based on their crystal and electronic structures.

Oxide semiconductors like ZnO, TiO_2 and SnO_2 have attracted considerable research interest over the last few years as these are proven to be multifunctional materials. These are basic materials, which have applications in various fields of optical and electronic devices [1]. Along with the optoelectronic device application, oxide-based materials are also found to exhibit multiferroic properties where both ferroelectricity as well as ferromagnetic order coexist. Tuning of optical, magnetic and ferroelectric properties along with semiconducting properties at room temperature (RT) is essential for the numerous novel applications preferably in a single-phase compound. Up to now, there are a very few reports on the observation of room-temperature multiferroics in oxide semiconductors. These properties have been observed by Lin et al. [2] in Li- and Co-doped ZnO films and Yang et al. [3] in Cr-doped ZnO thin films. More research efforts are being made in this direction. However, the observation of multiferroics at RT in ZnO and enhancement in the saturation values by non-metal–ion dopants will be an important step in terms of fundamental understanding and novel applications. ZnO is known to have hexagonal wurtzite structure which lacks the centre of symmetry and, hence, one expects ZnO to exhibit ferroelectric behaviour [4]. The origin and observation of magnetism in semiconducting materials like ZnO, GaN etc. has been debated. Earlier, the origin of magnetisation was thought to be associated with the transition metal ion doping. However, the observation of ferromagnetism at RT in undoped and non-metal-doped ZnO changed such understanding [5, 6]. In particular, defects like Zn and O vacancies, Zn interstitials, grain boundaries and lattice distortions are found to govern the magnetic ordering in oxide semiconductors. The origin of magnetism in these oxides is also commonly referred to as 'd^0-ferromagnetism'. Many theoretical as well as experimental studies resulted in limited understanding about the possible mechanism. The origin of magnetism in case of nanoparticles and thin films is supposed to be related with the reduced size effect, giving rise to the emphasis on the surface properties, or due to secondary phase after

P. Kumar · H.K. Malik
Department of Physics, Indian Institute of Technology Delhi, New Delhi 110016, India

H.K. Malik
e-mail: hkmalik@physics.iitd.ac.in

Y. Kumar · K. Asokan (✉)
Materials Science Division, Inter University Accelerator Centre, New Delhi 110067, India
e-mail: asokan@iuac.res.in

S. Annapoorni
Department of Physics & Astrophysics, Delhi University, New Delhi 110007, India

S. Gautam · K.H. Chae
Advanced Analysis Center, Korea Institute of Science and Technology (KIST), Seoul 136-791, Republic of Korea

transition metal ion doping. The carrier exchange mediated and bound magnetic polaron mechanisms are used to understand the defect-induced magnetism in the semiconductors [7]. Besides this, the ferromagnetism in case of these oxides also depends upon the synthesis techniques. However, the observations of ferromagnetism in bulk materials raise the controversy about the origin of magnetism in the oxide semiconductors. Up to now, magnetism has been reported in those systems where synthesis routes are followed by wet chemical methods and thin-film technologies. These methods, especially chemical methods, may have the presence of chemically absorbed moisture, nitrates and carbon, as some organic medium is required for these methods. The present study employs a conventional solid state reaction method for the preparation of Mg-doped ZnO at dilute concentration. Since these properties are basically related to the electronic structures of materials, one needs to use spectroscopic probes like near-edge X-ray absorption structure (NEXAFS), which is an effective experimental technique to know the sensitive nature of bonding between cations and anions. The NEXAFS at the O K-edge arises mainly due to the transition of O 1s electrons to the conduction band near the Fermi surface, which is dominated by the O 2p and transition metal hybridised 3d orbitals.

The present study focuses on the structural, magnetic, ferroelectric and electronic properties of dilutely Mg doped ZnO samples. $Zn_{1-x}Mg_xO$ ($0 \leq x \leq 0.05$) samples were synthesised using a solid state reaction method. The stoichiometric amounts of ZnO and MgO (99.99 % purity, Alfa Aesar) were mixed together and ground to obtain a uniform mixture. The samples were calcined at 800 °C for 6 h and sintered at the same temperature for 24 h to obtain the stable phase. X-ray diffraction (XRD) of the samples was carried out by a Bruker D8 Advance X-ray diffractometer using Cu-K_α (1.5414 Å) radiation. The magnetic measurements were carried out using a Microsense EV-9 vibrating sample magnetometer. Ferroelectric behaviour of the samples was examined by recording polarisations vs electric field loops at RT by a P–E loop tracer system (Marine India). NEXAFS measurements were done at the high energy spherical grating monochromator (HSGM) BL20A1 beam line in the National Synchrotron Radiation Research Centre, Hsinchu, Taiwan with 1.5 GeV energy and 360 mA storage ring current in top-up mode. All measurements were processed in an ultra high vacuum (UHV) chamber ($\sim 10^{-10}$ Torr) at 300 K. NEXAFS data were recorded in total electron yield (TEY).

Figure 1 shows the XRD patterns and their Rietveld refinements obtained with the help of FullProf software [8]. The Rietveld refinement was carried out with the space group P6$_3mc$ using a pseudo-Voigt function for the reflection profile of all the samples. In the refining process, wurtzite ZnO structure was selected as starting model structure and Mg ions were assumed to be incorporated into the

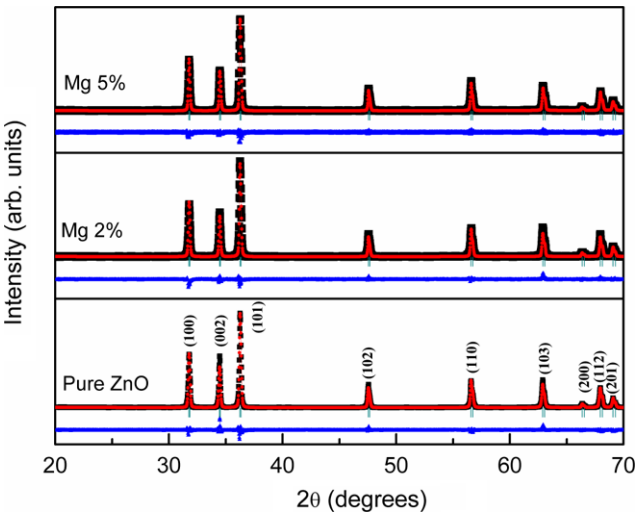

Fig. 1 XRD patterns with Rietveld refinements of $Zn_{1-x}Mg_xO$ ($x = 0, 0.02$ and 0.05) samples. Crystallinity is maintained with absence of impurity phases

ZnO lattice occupying Zn^{2+} sites. The characteristic peaks related to the impurities were not observed, confirming complete substitution of Mg into the host material. However, the (002) diffraction peak shifts towards higher scattering angle with the substitution of Mg in the ZnO lattice due to smaller ionic radius of Mg^{2+} ions (0.57 Å) as compared to that of Zn^{2+} ions (0.60 Å), resulting in compression of the unit cell. For pristine ZnO, the lattice parameters for a-axis and c-axis were found to be 3.249 Å and 5.203 Å, respectively, which is consistent with an earlier report on ZnO [9]. The lattice parameter c was observed to reduce and a to increase slightly ($\sim$0.05 Å) with doping concentration. The local wurtzite parameter ($u = a^2/3c^2 + 0.25$), which is the relative displacement between Zn and O sublattices along the c-axis, is found to increase and the c/a ratio to decrease with Mg concentration. It is known from the wurtzite structures that the c/a ratio deviates from the ideal value when the bonding character becomes more ionic [10]. The bond length (Zn–O) is found to reduce with the enhanced Mg content from 0 to 0.05. This small structural distortion caused by the bond-length variation is likely to drive the ferroelectric behaviour in $Zn_{1-x}Mg_xO$ systems.

Figure 2 shows the magnetic hysteresis curves measured at RT for Mg-doped ZnO samples. The M–H curve of all the samples exhibits a ferromagnetic feature. For ZnO, the saturation magnetisation (M_s) value is found to be $\sim 2 \times 10^{-4}$ emu/g at RT, which is consistent with previous reports on ZnO, TiO_2, In_2O_3 and HfO_2 [11, 12]. The origin of magnetisation in these oxides is associated with various kinds of defects present in the system. Oxygen vacancies (O_v) are the prominent defects, which give rise to the magnetisation in oxide semiconductors. As is evident from the graph, the value of saturation magnetisation (M_s) increases

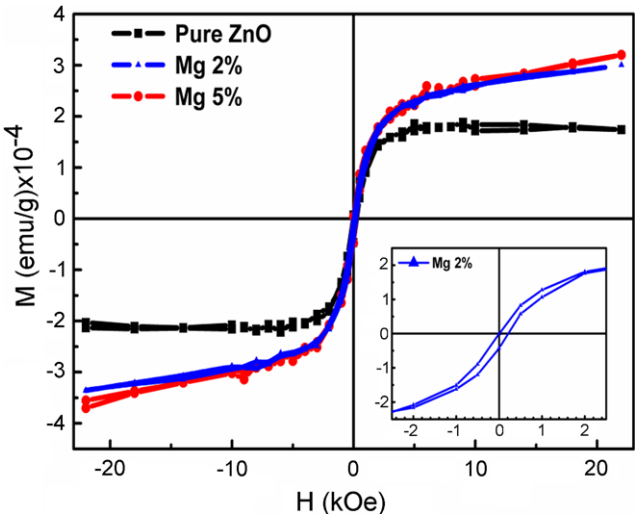

Fig. 2 Magnetisation curves for ZnO and Mg-doped ZnO. *Inset* shows the ferromagnetic behaviour of 2 % Mg doped ZnO

to 3×10^{-4} emu/g for 2 % Mg content, implying that M_s is closely associated with the Mg dopant. However, the value of magnetisation observed in the present case is small as compared to that of thin films and nanomaterials [13, 14]. The value of magnetisation for bulk samples in our case is 2×10^{-4} emu/g, which is about two orders less than the case of thin films/nanoparticles (0.05 emu/g for nanoflowers and 1.5×10^{-2} emu/g for thin films) [15, 16]. Doping of Mg in ZnO, which is a non-metallic dopant, has a significant effect on magnetisation at dilute doping concentration. Furthermore, the magnetic properties are tailored by Mg doping in ZnO, because the introduction of Mg on the Zn site introduces the lattice defects, in particular O_v.

The existence of ferroelectric nature in $Zn_{1-x}Mg_xO$ samples is confirmed by polarisation hysteresis curves, as shown in Fig. 3. The values of remanent polarisation (P_r) and coercive field (E_c) for pristine ZnO were found to be 0.5 μC/cm^2 and 4 kV/cm. A similar type of ferroelectric behaviour is also reported for Li- and Mg-doped ZnO samples [17, 18]. It can be seen from the graph that the remanent polarisation value increases (1.34 μC/cm^2) with the incorporation of Mg on the Zn site. The increase in the value is attributed to the difference in ionic radii of the dopant Mg^{2+} ions as compared to host Zn^{2+} ions. When Mg^{2+} ions replace the host Zn^{2+} ions, this causes a structural distortion induced along the polar *c*-axis. The ionic mismatch between Mg and Zn ions causes Mg to occupy an off-centred position, giving rise to an electric dipole moment. Moreover, from first-principle studies and the electronic configuration, it was found that Mg contains no 3*d* electron [19, 20]. While replacing Zn, it will enhance the ionic character and change the Zn–O bond length along the polar *c*-axis, resulting in a small structural distortion. If one considers the electronegativities of Mg and Zn, doping with Mg increases the ionic

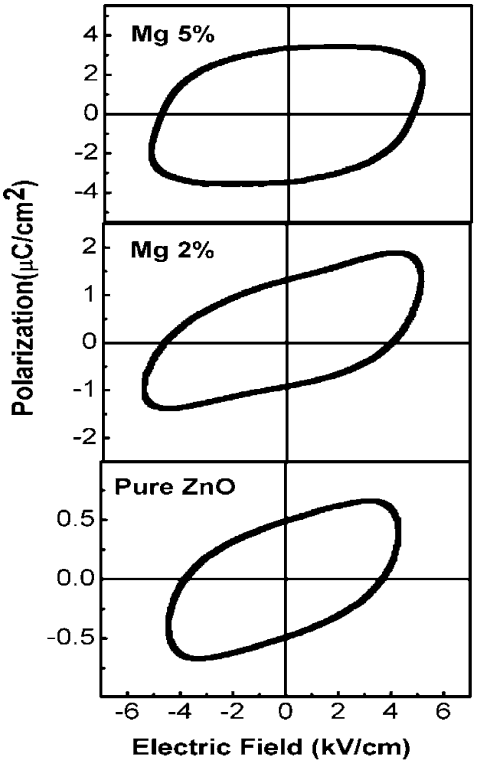

Fig. 3 Ferroelectric loop curves for $Zn_{1-x}Mg_xO$ samples. Pristine ZnO shows a weak ferroelectric nature compared to Mg-doped ZnO

character due to smaller electronegativity of Mg than Zn and gives rise to lattice distortion. Evidently, the P–E loop does not saturate, implying that ferroelectric character in case of ZnO is present but relatively small compared to $BaTiO_3$.

NEXAFS O K-edge spectra in transition-metal oxides provide the information about the hybridisation between O 2p electrons and transition-metal 3d electrons [21]. Figure 4 portrays the normalised NEXAFS spectra at the O K-edge of $Zn_{1-x}Mg_xO$ samples in total electron yield (TEY) mode. Based on existing literature and band-structure calculations, the various features in O K-edge spectra of ZnO are found to arise due to the transition of electrons from occupied 1s states to unoccupied 2p-derived states. These are obtained by hybridisation of O 2p orbitals with Zn 4s and 4p electrons, as there are no empty 3d states in Zn. The broad spectral features in the energy range 527–536 eV (peaks A and B) correspond to the hybridisation of O 2p with the highly dispersive Zn 4s states, thus forming the bottom of the conduction band. The features in the energy range 536–544 eV (peaks C, D and E) are due to the hybridisation of the O 2p states with the Zn 4p states. Above 544 eV, the features arise due to the O 2p states that extend to Zn higher orbitals. The observed O K-edge spectrum of the ZnO sample is similar to that of previous studies [22, 23]. Further, the spectral features of the NEXAFS O K-edge of $Zn_{1-x}Mg_xO$ samples are very similar to those of pristine ZnO samples. However, there is a reduction in the intensities of all the

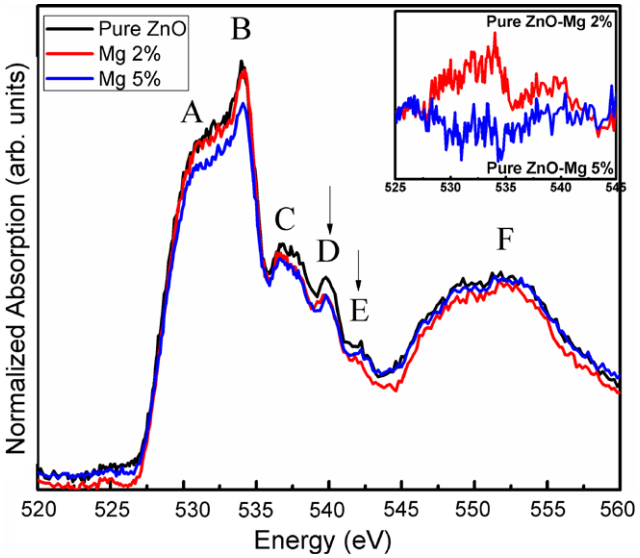

Fig. 4 Near-edge X-ray absorption fine spectra for $Zn_{1-x}Mg_xO$ samples at O K-edge. *Inset* shows the difference spectra of pristine ZnO–Mg 2 % and pristine ZnO–Mg 5 % samples

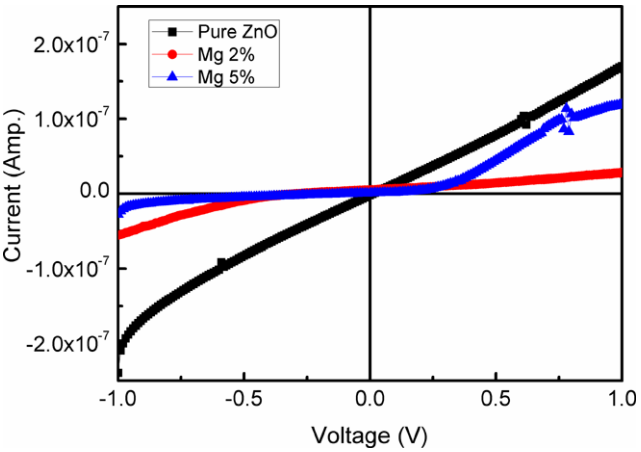

Fig. 5 I–V characteristic curves for Mg-doped ZnO samples

peaks observed for Mg-doped ZnO samples. The decrease in overall peak intensities is related to the reduction in the number of unoccupied O $2p$-derived states. The occupation of O $2p$ orbitals or further increase in the number of electrons in O ions with the increase in Mg content may be attributed to the smaller electronegativity of Mg (1.31 eV) as compared to Zn (1.65 eV). Mg doping causes the effective transfer of electrons to the O site, resulting in the reduction of unoccupied $2p$ states. The smaller electronegativity of Mg increases the ionic character of $Zn_{1-x}Mg_xO$ alloys, which in turn is responsible for the enhanced polarisation of doped samples. These results are in accordance with the results obtained from XRD and ferroelectric measurements.

During high-temperature sintering of ZnO, O ions are volatilised from host ZnO, resulting in dissociation of O ions, causing O vacancies (O_v) and Zn vacancies (Zn_v) [16]. These are the two dominating defects in ZnO, which are considered to be the possible origin of the magnetism. Doping Mg in ZnO even in dilute concentration enhances the non-centrosymmetrical crystalline structure of wurtzite ZnO. Since polarity is an intrinsic property for these structures, it induces a spontaneous polarisation within the cell. This leads to an internal electrical field, the amplitude of which directly depends on the relative positioning of the atoms in the unit cell and, therefore, on the lattice parameters. Presence of O defects acts in creating this multiferroic behaviour. Krishnamurthy et al. [24] understood the origin of magnetism in pristine ZnO thin films on the basis of O vacancies due to the presence of peaks at 538–544 eV (peaks D and E in our case) in NEXAFS spectra. In view of this and the peaks D and E in our case (Fig. 4), oxygen vacancies seem to be the origin of magnetism in the samples. Our previous study had indicated that O vacancies are enhanced with the higher doping of Mg (PL spectra in Ref. [9]). Hence, doping of Mg would create more defects, particularly O vacancies, in the system and this leads to higher magnetisation. On the other hand, due to the large band gap of MgO (7.7 eV), Mg doping increases the resistivity of host ZnO [25, 26] as observed by the increase in optical band gap of ZnO after Mg incorporation [9]. In order to further confirm the change in resistivity after Mg doping, I–V measurements for these samples were performed, which are shown in Fig. 5. In this figure, non-linearity of the I–V curves is found to increase with increasing Mg concentration. A similar effect has also been observed for multiferroic $LuFe_2O_4$ [27]. These curves depict the increase in resistivity after Mg doping. It may be contemplated that the presence of Mg doping leads to localisation of charge carriers increasing the resistance of the materials. The values of resistance obtained after linear fitting of these curves are found to be 0.6×10^7 Ω, 3.5×10^7 Ω and 6.6×10^7 Ω. Enhancement in resistivity with Mg doping in ZnO is a general behaviour of the Mg-doped samples and is consistent with the previous studies. Higher resistivity of Mg-doped samples reduces the leakage current and favours the ferroelectric nature [28]. Also, due to the difference in ionic radii of the two ions (Zn^{2+} and Mg^{2+}), the lattice distortion takes place that also contributes to the ferroelectric behaviour. Even though the signal of ferroelectricity is weak, it is not negligible, which gives rise to many issues related to multiferroic nature in d^0 systems. This is fundamentally important to understand the origin of such complex manifestations in nature.

The coexistence of RT single-phase multiferroics is very much limited so far. The ferroelectricity and ferromagnetism have been independently studied in ZnO-based systems long before. However, the observed value of ferroelectric behaviour in the present case is small as compared to highly ferroelectric materials like Zr-doped $PbTiO_3$ and $BiFeO_3$ [29]. In the present study, the bond length reduces

with the Mg incorporation that causes off-centred distortion and results in the dipole moment. Hence, on the basis of existing literature as well as the present indications, the existence of ferroelectric nature in these samples cannot be ignored even though similar $P-E$ loops to those shown are easily obtained on lossy dielectrics [30, 31]. However, more research efforts need to be made in this direction for the improvement of ferroelectric nature. The coexistence of both ferromagnetic and ferroelectric nature at RT implies the need for a new outlook in understanding the condensed matter theory. Some of the exclusive nature identified by the present theory has been proved to be inclusive. Critical examination implies the need for microscopic understanding of the density of electronic states and how this gets modified due to defects and, hence, influences magnetic and electric transitions. Therefore, the observed multiferroic nature at room temperature demonstrates another dimension towards multifunctionality of ZnO for its possible application to material and device designing in the near future.

Acknowledgements The authors would like to thank IUAC, New Delhi for the XRD facility and Dr. Anurag Gaur, NIT Kurukshetra and Ms. Rekha Gupta, research scholar, Delhi University for their help during the experiment. The authors S.G. and K.H.C. are thankful to Prof. J.M. Chen (NSRRC) for the synchrotron experimental support and discussions. One of us (K.A.) acknowledges the financial support of DST under the Indo–Russian project No. INTRFBR/P-72.

References

1. U. Ozgur, Ya.I. Alivov, C. Liu, A. Teke, M.A. Reshchikov, S. Dogan, V. Avrutin, S.J. Cho, H. Morkoc, J. Appl. Phys. **98**, 041301 (2005)
2. Y.H. Lin, M. Ying, M. Li, X. Wang, C.W. Nan, Appl. Phys. Lett. **90**, 222110 (2007)
3. Y.C. Yang, C.F. Zhong, X.H. Wang, B. He, S.Q. Wei, F. Zeng, F. Pan, J. Appl. Phys. **104**, 064102 (2008)
4. S. Hagino, K. Yoshio, T. Yamazaki, H. Satoh, K. Matsuki, A. Onodera, Ferroelectrics **264**, 232 (2001)
5. J.M.D. Coey, Solid State Sci. **7**, 660 (2005)
6. J.M.D. Coey, M. Venkatesan, C.B. Fitzgerald, Nat. Mater. **4**, 173 (2005)
7. Y. Li, R. Deng, B. Yao, G. Xing, D. Wang, T. Wu, Appl. Phys. Lett. **97**, 102506 (2010)
8. J. Rodriguez-Carvajal, FULLPROF—a program for Rietveld refinement. Laboratoire Leon Brillouin, CEA-Saclay, France, 2000
9. P. Kumar, J.P. Singh, Y. Kumar, A. Gaur, H.K. Malik, K. Asokan, Curr. Appl. Phys. **12**, 1166 (2012)
10. Y. Kim, K. Page, R. Seshadric, Appl. Phys. Lett. **90**, 101904 (2007)
11. N.H. Hong, J. Sakai, N. Poirot, V. Brizé, Phys. Rev. B **73**, 132404 (2006)
12. N.H. Hong, N. Poirot, J. Sakai, Appl. Phys. Lett. **89**, 042503 (2006)
13. X. Xu, C. Xu, J. Dai, J. Hu, F. Li, S. Zhang, J. Phys. Chem. C **116**, 8813 (2012)
14. P. Zhan, W. Wang, Q. Xie, Z. Li, Z. Zhang, J. Appl. Phys. **111**, 103524 (2012)
15. X. Bie, C. Wang, H. Ehrenberg, Y. Wei, G. Chen, X. Meng, G. Zou, F. Du, Solid State Sci. **12**, 1364 (2010)
16. M. Khalid, M. Ziese, A. Setzer, P. Esquinazi, M. Lorenz, H. Hochmuth, M. Grundmann, D. Spemann, T. Butz, G. Brauer, W. Anwand, G. Fischer, W.A. Adeagbo, W. Hergert, A. Ernst, Phys. Rev. B **80**, 035331 (2009)
17. A. Onodera, N. Tamaki, Y. Kawamura, T. Sawada, B. Yamashita, Jpn. J. Appl. Phys. **35**, 5160 (1996)
18. Dhananjay, S. Singh, J. Nagaraju, S.B. Krupanidhi, Appl. Phys. A **88**, 421 (2007)
19. A. Onodera, N. Tamaki, K. Jin, H. Yamashita, Jpn. J. Appl. Phys. **36**, 6008 (1997)
20. Dhananjay, J. Nagaraju, S.B. Krupanidhi, J. Appl. Phys. **99**, 034105 (2006)
21. E. Kisi, M.M. Elcombe, Acta Crystallogr., Sect. C **45**, 1867 (1989)
22. J.W. Chiou, H.M. Tsai, C.W. Pao, K.P.K. Kumar, S.C. Ray, F.Z. Chien, W.F. Pong, M.H. Tsai, C.H. Chen, H.J. Lin, J.J. Wu, M.-H. Yang, S.C. Liu, H.H. Chiang, C.W. Chen, Appl. Phys. Lett. **89**, 043121 (2006)
23. J.W. Chiou, H.M. Tsai, C.W. Pao, F.Z. Chien, W.F. Pong, C.W. Chen, M.H. Tsai, J.J. Wu, C.H. Ko, H.H. Chiang, H.J. Lin, J.F. Lee, J.H. Guo, J. Appl. Phys. **104**, 013709 (2008)
24. S. Krishnamurthy, C. McGuinness, L.S. Dorneles, M. Venkatesan, J.M.D. Coey, J.G. Lunney, C.H. Patterson, K.E. Smith, T. Learmonth, P.A. Glans, T. Schmitt, J.H. Guo, J. Appl. Phys. **99**, 08M111 (2006)
25. N. Kılınç, L. Arda, S. Ozturk, Z.Z. Ozturk, Cryst. Res. Technol. **45**, 529 (2010)
26. K. Huang, Z. Tang, L. Zhang, J. Yu, J. Lv, X. Liu, F. Liu, Appl. Surf. Sci. **258**, 3710 (2012)
27. B. Fisher, J. Genosser, L. Patlogan, G.M. Reisner, J. Appl. Phys. **109**, 084111 (2011)
28. T.S. Herng, M.F. Wong, D. Qi, J. Yi, A. Kumar, A. Huang, F.C. Kartawidjaja, S. Smadici, P. Abbamonte, C. Sánchez-Hanke, S. Shannigrahi, J.M. Xue, J. Wang, Y.P. Feng, A. Rusydi, K. Zeng, J. Ding, Adv. Mater. **23**, 1635 (2011)
29. G. Catalan, J.F. Scott, Adv. Mater. **21**, 2463 (2009)
30. J.F. Scott, J. Phys. Condens. Matter **20**, 021001 (2008)
31. A. Soukiassian, A. Tagantsev, N. Setter, Appl. Phys. Lett. **97**, 192903 (2010)